J Mater Sci (2012) 47:289–298
DOI 10.1007/s10853-011-5797-9

Synthesis and characterization of smoke-like porous sol–gel indium tin oxide coatings on glass

Nilanjana Das · Prasanta Kumar Biswas

Received: 18 February 2011 / Accepted: 15 July 2011 / Published online: 29 July 2011

Abstract A precursor for porous indium tin oxide (ITO) coatings with smoke-like surface feature was prepared from the hydrated metal [In(III)/Sn(IV)] salts and polyvinyl alcohol (PVA) solvated in a mixed aqueous-organic medium. Films were prepared by dip coating and cured at four temperatures (60 °C, 150 °C, 250 °C and 400 °C) where different surface features and morphological properties were obtained. The thickness of the films ranged from 0.5 to 1.2 μm. After the 60 °C cure, the surface showed a unique "smoke-like" feature of combustion products of PVA-ITO precursor. Increasing the cure temperature to 150 °C led to the development of In(III) and Sn(IV) moieties incorporated in crystalline PVA having the shape close to the hexagonal. Study of thermogravimetric analysis and differential thermal analysis of the material suggests that the gel to oxide transformation occurs by the removal of physisorbed water, PVA and nitrate ion followed by the condensation of hydroxide groups. Electrical parameters such as resistivity, conductivity, sheet resistance were evaluated by two- and four-point probe methods. Field emission scanning electron microscopy and transmission electron microscopy studies of the sample cured at 400 °C showed that the films were a porous network containing 5–40 nm clusters of ITO.

Introduction

Indium tin oxide (ITO), a wide band gap semiconductor is one of the intensively investigated post-transition metal oxides because of its promising electrical and optical properties. It has versatile applications in thin film/bulk form in the areas of electrochromic devices [1], flat panel displays [2], organic light emitting diodes (OLEDs) [3], thin film transistors (TFTs) [4], electrocatalysis [5], photocatalysis [6], non-linear optics [7], acoustic insulation [8], adsorption of environmental pollutants [6], biotechnology for cell labelling and imaging [9, 10], etc. Indium tin oxide (ITO) is essentially formed by substitutional doping in In_2O_3 with tin [Sn (IV)] which replaces the In (III) in cubic bixbyite structure of In_2O_3 giving rise to the formation of a n-type semiconductor possessing high electrical conductivity. It is transparent conducting oxide (TCO) of indium and tin in thin film form which is used as a transparent electrode in various electronic devices [1–4, 7]. Presently researchers are also involved in finding out porous network of semiconductors as followed for ZnO, TiO_2 systems for their specific applications in the areas of photocatalysis, dye sensitised solar cells, etc., where stable porous network should be maintained in films [11–13]. However, a wonderful application of porous ITO in the fabrication of porous electrode has been reported [14, 15].

In this article, our main objective is to focus on easy fabrication of porous ITO network in the film form for similar applications as described above. We are reporting here the synthesis and characterization of smoke-like ITO gel-film leading to porous network. In most cases, ITO is produced in the form of thin films by the application of various methods such as magnetron sputtering [16, 17], pulsed laser deposition [18], chemical vapour deposition [19] and spray pyrolysis [20]. However, these techniques are highly restricted with respect to processing for substrate geometry. Therefore, liquid phase processing of ITO thin films became a widely applied alternative as this technique is independent of substrate geometry [21, 22]. In addition, cost effective sol–gel

N. Das · P. K. Biswas (✉)
Sol-Gel Division, CSIR-Central Glass and Ceramic Research Institute, 196 Raja S.C. Mullick Road, Jadavpur, Kolkata 700 032, India
e-mail: pkbiswas@cgcri.res.in

dipping/spinning approach is highly successful in the preparation of ITO coatings [7, 23] on glass. Sol–gel technique also allows the control of porosity of the films by utilization of appropriate microstructure directing agent. As a result, this simple and highly advantageous sol–gel method is employed here for the preparation of porous coatings.

Experimental procedure

Preparation of precursor

The hydrated indium nitrate solution was synthesized starting with indium (In) metal ingots (99.99%, SRL, India) and conc. nitric acid (GR grade, E. Merck, India). Initially requisite amount of indium nitrate solution was taken for the preparation of precursor. The mixed aqueous-organic-based precursor sol of ITO (6 wt% equivalent metal oxides, In:Sn = 90:10, at.%) was prepared by adding hydrated stannic chloride ($SnCl_4 \cdot 5H_2O$, 98%, Loba Chemie) to the above prepared hydrated indium nitrate solution. Next suitable amount of polyvinylalcohol (PVA) (molecular weight 22000, BDH, UK) was used as an organic binder to increase the stability of the precursor sol. The sol was aged for a few days before using for coating. A Schematic diagram (Fig. 1) of various steps required for precursor preparation will reveal the procedure more clearly.

Deposition of coating onto glass substrate

The above precursor was used for the deposition of layers onto the cleaned bare soda lime silica glass (dimensions 25 × 75 mm^2) by dip coating technique [Chemat make Dip Master 200, USA] with specific withdrawal speed of 16 cm/min in 10,000-class clean air room equipped with 100 class work station. The coated sample was placed in an air oven and heated to 60 °C for 30 min leading to the formation of smoke-like gel layer. This film was further put into an electrical furnace and cured in air at different temperatures, 150° ± 5 °C, 250° ± 5 °C and 400° ± 5 °C with 30 min soaking in each case. We designate the samples as ITO-60, ITO-150, ITO-250 and ITO-400 according to the curing at 60 °C, 150 °C, 250 °C and 400 °C, respectively. The whole process of preparation of precursor and the coating thereof is shown in Fig. 1.

Characterization

Physical thickness and refractive index (at 632.8 nm) of the coatings was measured ellipsometrically (Gaertner make Autogain L116B, USA) using He–Ne laser of 632.8 nm wavelength. To investigate surface roughness with respect to physical thickness, the data were measured at different

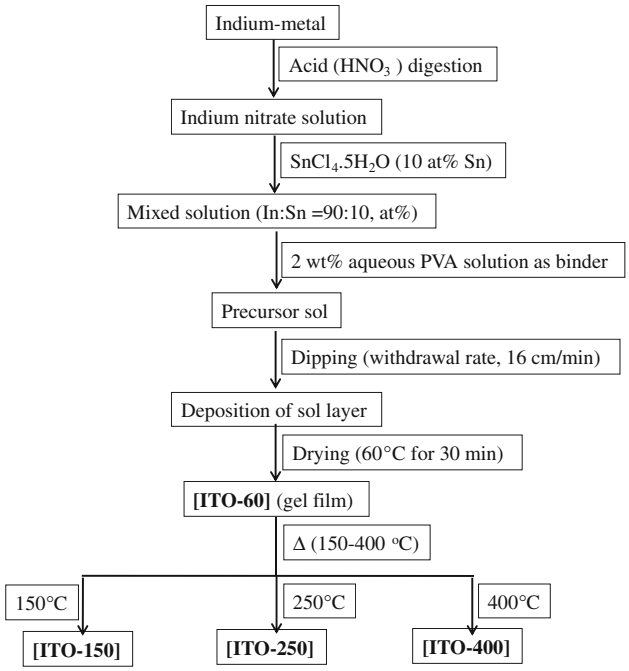

Fig. 1 Schematic representation for the processing of smoke-like ITO films

points with an interval of 2 mm gap along the *x*- and *y*- directions. For this, the specimen size of the surface was chosen as 10 × 10 mm^2. Thus multiple data sets for the measurement at twenty different points were collected for each sample and average (mean) thickness values along with standard deviations for all the specimens are depicted in Table 1. Thermal characteristics [thermogravimetric analysis (TGA) and differential thermal analysis (DTA)] of the gel to oxide transformation in the gel film was carried out by using a Netzsch STA 409 C/CD Thermoanalyzer with Al_2O_3 as a reference material maintaining heating rate of 10 K/min in air. The chosen maximum temperature was 1350 °C. Practically the gel film (obtained after drying at ~60 °C) material (~20 mg obtained from a series of coated samples) was taken out from the surface of the substrate by scrubbing which was used as the starting material for TGA–DTA experiment. Crystalline phase was identified by X-ray diffractogram (XRD) obtained from an X-ray diffractometer [Philips PW 1730 X-ray diffraction unit employed with nickel-filtered CuK_α radiation source (1.5418 Å radiation)]. The diffraction angle was chosen from 10 to 70° with continuous scanning at a rate of 0.6°/min. The transmission spectra were measured by UV–VIS-NIR spectrophotometer (Shimadzu make UV-PC-3100, Japan). The double beam scanning was used for the measurement in the wavelength range from 200 to 2500 nm (photometric accuracy; ± 0.3%, resolution, 0.10 nm). Surface morphology and the cluster size distribution of nanostructured indium tin oxide film were studied by field

emission scanning electron microscopy (FESEM) (ZEISS, SUPRA^{TM}35VP) and transmission electron microscopy (TEM) (TecnaiG^2 30.S-Twin, FEI Company, Netherlands), respectively. Carbon coated 300 mesh Cu grid was used for TEM images. The vacuum level for this experiment was around 10^{-9} Torr. For sample preparation, the films were scratched which were then dispersed in cyclohexane followed by sonication for about 2 h. Finally it was carefully placed on the Cu-grid. The excess liquid was allowed to evaporate in air. The grids with the sample were examined with ultra-high resolution (UHR) pole-piece using a LaB6 filament. The operated accelerating voltage and the camera length were 300 kV and 55 cm, respectively. FTIR spectra of the films were measured by Thermo Electron Corporation make Nicolet 5700 FTIR spectrometer. Number of scans for each experiment was 164 when the wavenumber resolution was 4 cm^{-1}. The sheet resistance of the films were measured by two probe method using a Philips (PM 2525) make multimeter. During the measurement, the sheet resistance was measured along the parallel and perpendicular directions of withdrawal operation of film deposition. The resistivity and conductivity were measured from the corresponding sheet resistance and physical thickness values. Electrical parameters (Tables 4 and 5) such as conductivity, carrier concentration, Hall mobility, resistivity and sheet resistance of a typical film prepared at 400 °C (ITO-400) were measured by four probe method utilizing EGK make Van der Pauw Hall effect measurement system (HEM 2000, South Korea) based on compact desk-top design where 0.51T magnetic field was used. Sheet resistance of the ITO-400 film was also evaluated from the knowledge of its resistivity and physical thickness values. Adhesion properties of the coatings were determined by Scotch ^{TM} Magic ^{TM} tape (imported by 3 M India Ltd.) test. Percentage (%) of transmission and reflection properties of the coatings at 550 nm were measured by UV–VIS-NIR spectrophotometer (Shimadzu make UV-PC-3100) before and after 100 times application of the 3 M- Scotch tape to understand any variation in optical properties. Variation of physical thickness (if any) due to the application of the tape was also noted ellipsometrically. Table 6 depicts the results of the adhesion test.

Results and discussion

Sol layer from polyvinyl alcohol (PVA)-based ITO precursor was cured at 60 °C when a smoke-like surface feature was obtained. The above surface feature can be retained even at higher temperatures such as 150 °C, 250 °C and 400 °C. The normal shrinkage behaviour was observed in the case of heating the sample, with an exception to the heat treatment at 150 °C. This was authenticated by the ellipsometric measurement of physical thickness which was verified by the cross sectional microstructural (FESEM) study. Homogeneity of each film was checked by the knowledge of thickness and refractive index at twenty different points. ITO-60 possesses average film thickness of ~578 nm over the area 1 × 1 cm^2. The average film thickness changes to 1214 nm (~1.2 μm), 365 nm and 251 nm, respectively, for curing the samples at 150 °C (ITO-150), 250 °C (ITO-250) and 400 °C (ITO-400), respectively (Table 1). In each case, standard deviation of film thickness over the area 1.0 × 1.0 cm^2 is within 5%, while for R.I. it is within 0.7% which supports homogeneity even after heat treatment.

Amorphous/crystalline nature of the specimens was identified by XRD (Fig. 2) study. The diffractogram of

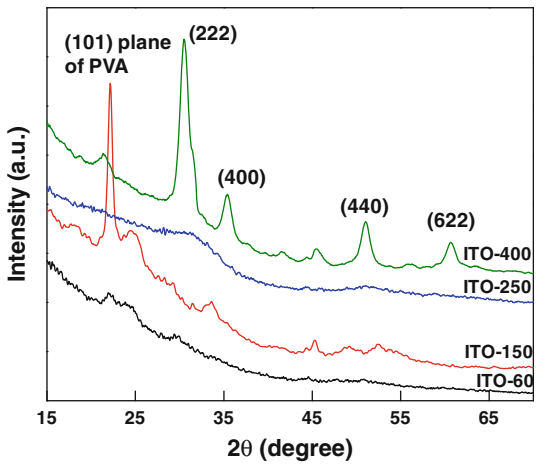

Fig. 2 XRD reflections of smoke-like ITO films at different temperatures

Table 1 Thickness, refractive index and percentage of standard deviations of the smoke-like ITO films obtained at different temperatures

Specimen	Physical thickness (nm)			Refractive index		
	Average value (nm)	Standard deviation	Standard deviation (%)	Average value	Standard deviation	Standard deviation (%)
ITO-60	578	18.20	3.149	1.406	0.007	0.498
ITO-150	1214	26.77	2.205	1.555	0.010	0.643
ITO-250	365	15.96	4.372	1.659	0.009	0.517
ITO-400	251	10.43	4.156	1.741	0.007	0.402

ITO-60 did not show crystallinity. This may be due to the gel-like structure of organic–inorganic layer. But the coating heated at ~150 °C (ITO-150) shows crystalline behaviour. The peak at $2\theta = \sim 20°$ corresponds to the (101) plane of undecomposed crystalline PVA having the unit cells close to hexagonal [24, 25] which has possibly led to the generation of hexagonal shape of the clusters as evident from the FESEM image (see below). However, Bunn [26] and Colvin [27] predicted the pseudo-orthorhombic and monoclinic structure of crystalline PVA. In this case, the diffraction lines of ITO are not well-resolved due to the presence of the organic moiety. However, the characteristic 2θ line for PVA is almost negligible in the case of ITO-250 since PVA decomposes at ~250 °C. However, we have observed small humps at $2\theta = \sim 30°$ and 50° due to the reflections from the planes (222) and (440) of bixbyite cubic structure of ITO. In ITO-400, all the diffraction lines in XRD pattern show distinct characteristic lines of the cubic structure [28] of ITO with close resemblance to oxygen deficient $In_2Sn_2O_{7-X}$ entities [29]. No separate peaks were observed for SnO_2, as the doping level of Sn (IV) in In_2O_3 was considerably low (10 at.%).

To understand the sequential steps of the transformation of smoke-like gel to oxide layer of ITO system, thermogravimetric analysis (TGA) was performed with the gel film material obtained by scrubbing the film material prepared at 60 °C (Fig. 3). The TGA depicts a total loss of 65.28% which takes place in five steps (*I–V*, as shown in Fig. 3) inferred from the appearance of five inflexions in the curve which would basically prefer a range of temperature. Finally, no weight loss was observed after a temperature of 550 °C when complete transformation to oxide form has occurred. As per the weight loss at the temperatures of inflexion points, a tentative formulation of

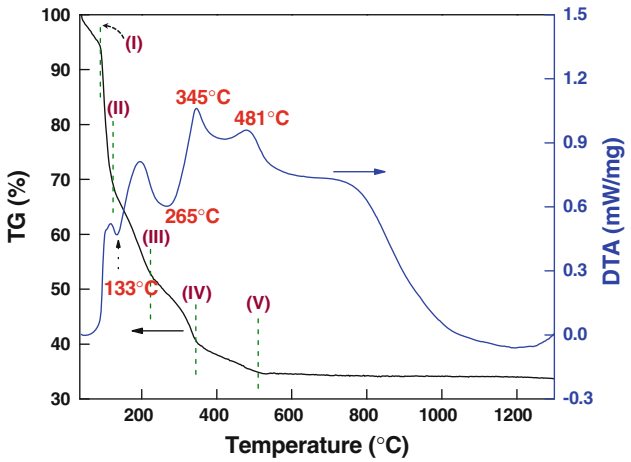

Fig. 3 DTA-TGA curves of smoke-like ITO film cured at 60 °C in air (ITO-60)

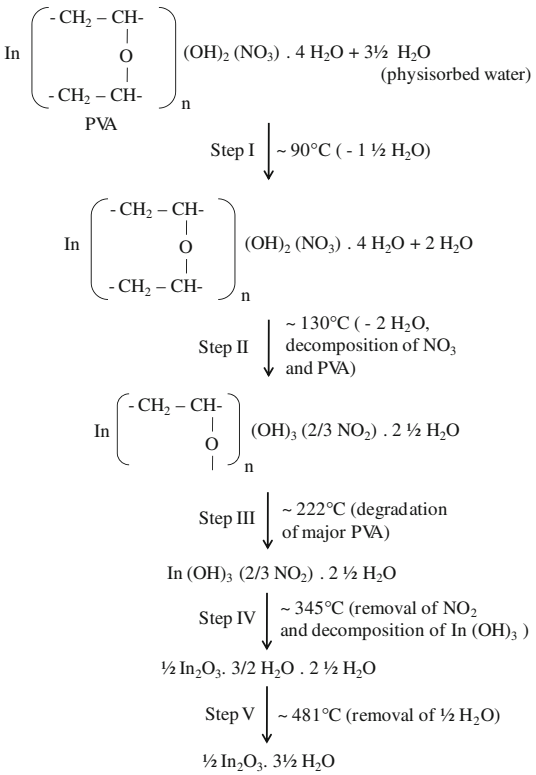

Scheme 1 Proposed steps of the gel to oxide transformation of ITO system

starting material along with the intermediate products may be proposed (Scheme 1) which was supported by the FTIR analysis (Fig. 4) of the products isolated at the temperatures near the inflexion point. At the initial stage cross linked PVA may be proposed for the presence of the

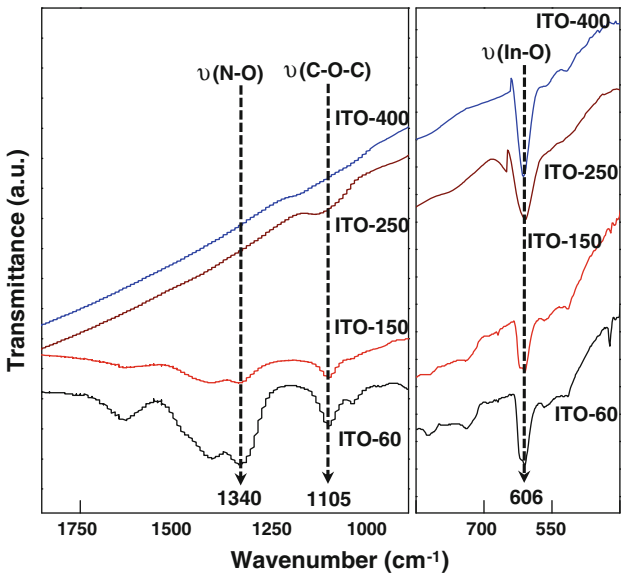

Fig. 4 FTIR spectra of smoke-like ITO films isolated at different temperatures

characteristic vibrational band [υ(C–O–C)] [30] at 1105 cm^{-1}. Co-ordination with water molecules cannot be nullified as there (not shown here) is a broad shoulder at ~3200 cm^{-1} for υ(O–H) which also exists for the heated samples. The differential thermal analysis (DTA) curve reveals a combination of exothermic and endothermic peaks. Initially two endothermic peaks were obtained followed by two exothermic peaks which are due to the evolution of physisorbed/chemisorbed water, decomposition of nitrate ion and PVA binder leading to the formation of metal oxide.

Detailed steps are: Step I (~90 °C) may be due to the loss of some physically adsorbed water molecules which is accompanied by Step II (~130 °C) for the loss of the remaining physically adsorbed water molecules [31], decomposition of nitrate ion and onset of degradation of the organic binder, PVA as evident from the decreasing intensity of the characteristic vibrational band [υ(C–O–C)] in the FTIR spectra of ITO-150. In this case, gaseous nitrogen dioxide (NO_2) molecules may be trapped after the decomposition of nitrate as evident from the presence of the characteristic vibrational band for υ (N–O) ~ 1340 cm^{-1} [32] in the FTIR spectra (Fig. 4). This was not found for ITO-250 indicating the removal of NO_2 at the initial stage of Step IV. In Step III (~222 °C), the major organic moiety is removed [33] with the dehydration of $In(OH)_3$ [34] as evident from the appearance of small hump due to υ(C–O–C) in the FTIR spectra for ITO-250. The above three steps may be responsible for the initial endothermic peaks in DTA. The exothermic peak and the weight loss in the range 345–400 °C (Step IV) are expected for the complete decomposition of $In(OH)_3$ to In_2O_3 [35, 36] with the complete burning of PVA as there is no hump for υ(C–O–C) in the FTIR of ITO-400 where the In-O stretching [37] vibration at ~600 cm^{-1} is more prominent. For Step V (~481 °C), water is evolved out which may be for more condensation between the hydroxyl groups of $In(OH)_3$ species. As per the Scheme 1, the calculated loss from Step I to Step V is 65.41% assuming $n = 1$ for the polymer entity, which is comparable with the result obtained from TG analysis (65.28%).

To determine the transmissivity of the smoke-like films, the transmission spectra were studied (Fig. 5). All the films were transparent in the visible region (60–82%), but the transparency increases in the near-IR region (800–2500 nm). Hence, it may be predicted that the ITO films of about 250–1200 nm would pass solar radiation considerably. The cross-sectional FESEM of ITO-60 (Fig. 6a) highlights the film thickness and the surface feature. Figure 6b is the magnified image of Fig. 6a depicting ~605 nm film thickness which is in agreement with the film thickness obtained ellipsometrically. A smoke-like evolution at the surface is also observed here. This smoke-like evolution of ITO

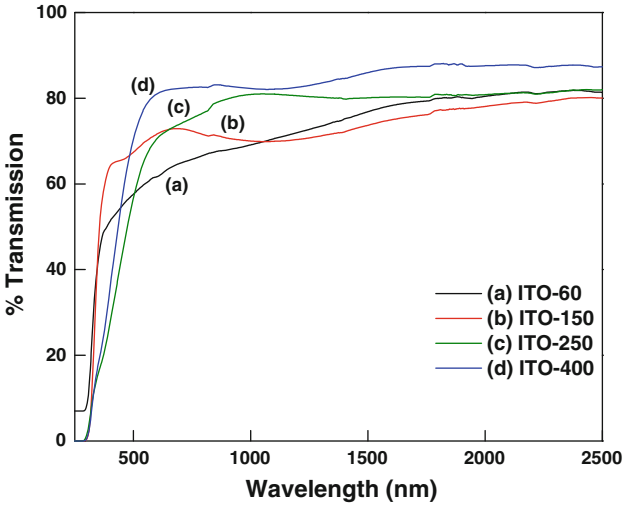

Fig. 5 Transmission spectra of smoke-like ITO films cured at different temperatures

precursor-based film has so far never been reported in literature. Figure 6c highlights the film surface of ITO-60 determined by FESEM study which illustrates the formation of organic–inorganic hybrid ITO clusters. The inset of the Fig. 6c shows the size distribution of the clusters as depicted by the histogram, the average size being ~162 nm.

It is to be noted that there are two specific functions of the organic binder, PVA. These are (i) to increase wettability of the precursor sol due to the presence of sufficient number of hydroxyl groups and (ii) to generate nanoclusters through the decomposition [7] of the crystalline shape of PVA-ITO system which has been formed at ~150 °C (Fig. 7a). The increase in thickness after heating of ITO-60 is possibly due to the formation of crystalline PVA clusters of ~1 μm size (inset of Fig. 7a, highlighting the histogram of size distribution, average cluster size ~831 nm) containing the moiety of In (III) and Sn (IV) metals. Figure 7b is the magnified image of Fig. 7a where the crystalline shape of PVA crystals containing the In (III) and Sn (IV) moiety is highlighted. Owing to the formation of these grains of larger dimensions, the thickness of ITO-150 increases (Table 1) with increase in temperature which is also supported by the cross-sectional FESEM (Fig. 7c) study. This Figure also indicates the retention of the smoke-like nature of the film even at 150 °C. Porous nature of the film is clear in the FESEM and TEM images, but the TEM image clearly explains the distribution of pores (Fig. 8a). A little magnification of the image shows the tube-like arrangements of the pores present in the PVA-ITO-based matrix (Fig. 8b). The EDS study (Table 2) indicates In:Sn (at%) = ~ (95:05) inspite of 90:10 (starting composition) due to the presence of high percentage of carbon of PVA. The exact percentage of carbon

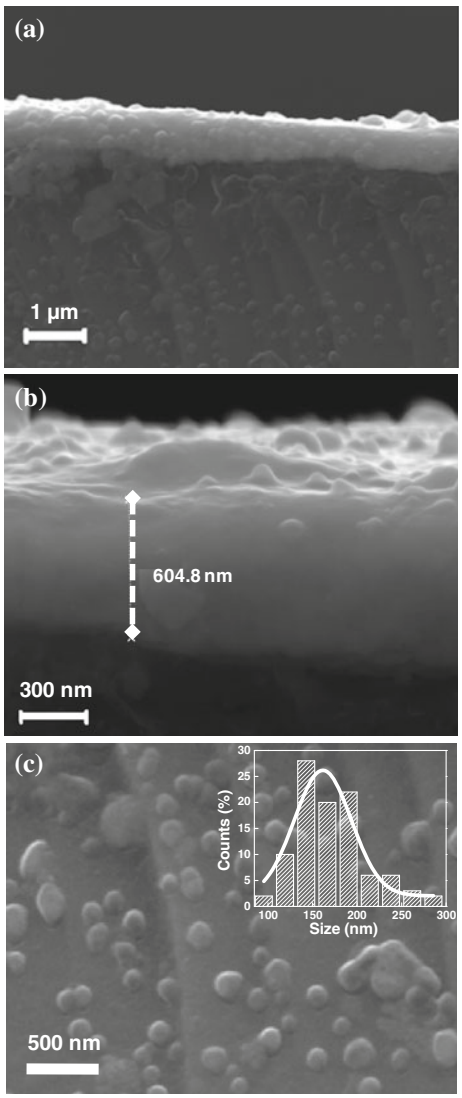

Fig. 6 **a** Cross-sectional FESEM image of ITO-60; **b** magnified image of **a** highlighting smoke-like surface; **c** FESEM image of the film surface of ITO-60; *inset* shows histogram of particle size distribution with average size of ~162 nm

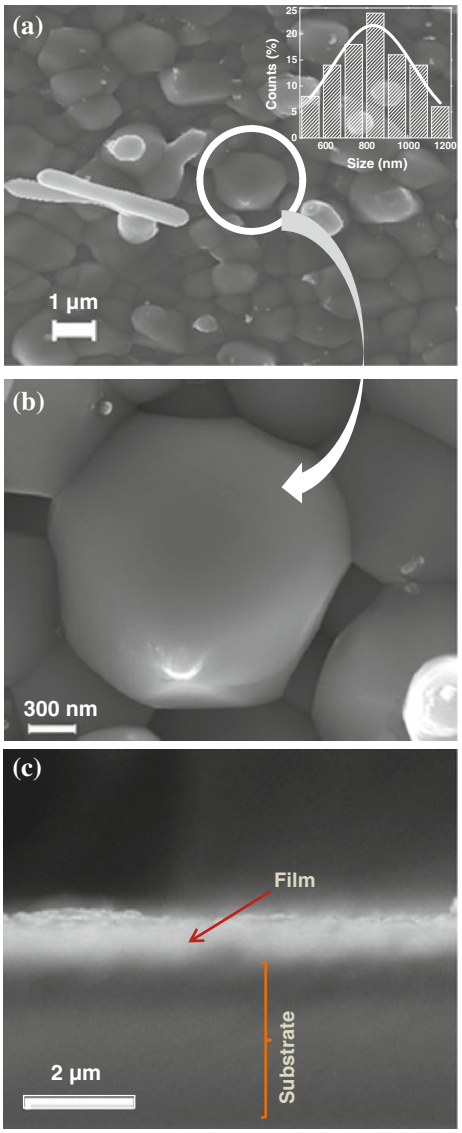

Fig. 7 **a** FESEM image of the film surface of ITO-150; *inset* shows histogram of particle size distribution with average size of ~831 nm; **b** image of **a** at higher magnification highlighting a single grain; **c** Cross-sectional FESEM image of smoke-like ITO-150

could not be determined here due to the usage of carbon-coated grid in TEM experiment.

With the increase in curing temperature to 250 °C, major decomposition of PVA occurs. At this stage, major PVA disappeared (confirmed by the FTIR study mentioned above). As a result, the film thickness decreases to ~365 nm. This is confirmed by both ellipsometry (Table 1) and cross-sectional FESEM studies of the film (ITO-250) (Fig. 9a). Presence of smoke-like nature still exists. Figure 9b describes the FESEM at higher magnification which shows that small ITO particles are formed. The inset of Fig. 9b shows the histogram of the size distributions; the average particle size is ~71 nm where the particles are more or less evenly distributed in the film matrix.

It was also observed that when the coating was cured at 400 °C (ITO-400), ITO nano-clusters are generated. This is evident from the FESEM image (Fig. 10a). The average cluster size as determined from the histogram of size distributions is ~40 nm (inset of Fig. 10a). The smoke-like film thickness decreases to ~250 nm due to removal of PVA determined from the cross-sectional FESEM (Fig. 10b), which is also confirmed (~251 nm) ellipsometrically (Table 1). The TEM image (Fig. 10c) also confirms the generation of ITO nanoclusters. This image has also been utilized to estimate the nanocluster size of ITO. The average size of ~9 nm diameter was obtained from the size distribution of the clusters depicted in the histogram (inset of Fig. 10c). This is in agreement with the

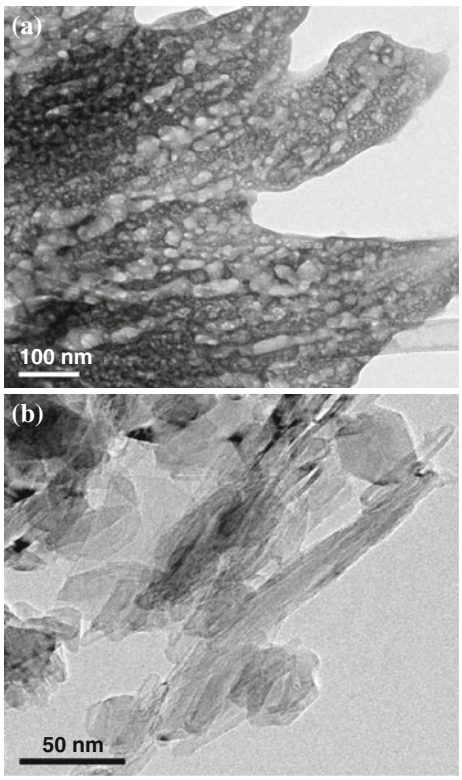

Fig. 8 **a** TEM image of ITO-150 showing distribution of pores; **b** TEM image of ITO-150 showing alignment of pores

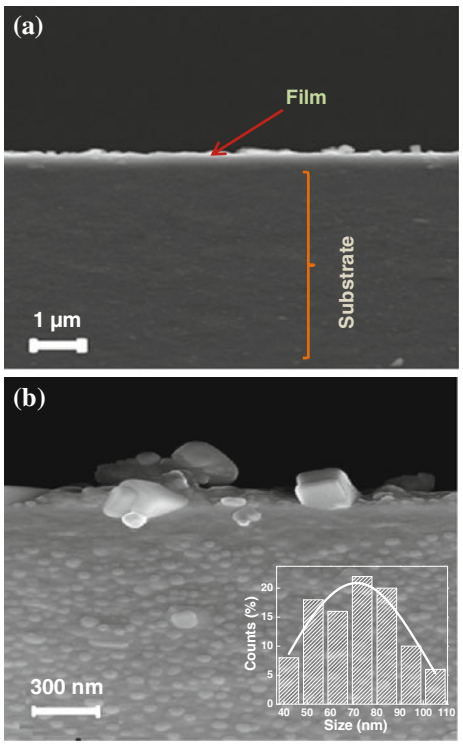

Fig. 9 **a** Cross-sectional FESEM image of ITO-250; **b** Surface feature of ITO-250; *inset* shows histogram of particle size distribution with average size of ~71 nm

Table 2 In:Sn in at.% evaluated from TEM-based EDS spectra of the smoke-like ITO films heated at 150 and 400 °C

Elements	ITO-150	ITO-400
In	95.7	89.1
Sn	4.3	10.9

particle size of 7.4 nm, as estimated from the ⟨222⟩ lattice plane (Fig. 10d) using Scherer's equation. The development of crystallinity is also confirmed from the ED pattern (inset of Fig. 10d). The EDS study (Table 5) confirms the composition of In:Sn (at.%) = 89.1:10.9, comparable with the starting composition, 90:10 taken in the precursor. In this case, the contribution of carbon due to PVA is negligible. As a result, it may be inferred that complete removal of PVA has occurred at this stage.

Dependence of cluster size on the curing temperature is illustrated by the plot (Fig. 10e) of cluster size against curing temperature. Development of nanoclusters of different sizes is highlighted through this curve. As TEM study did not help to locate the cluster size for all the specimens, the FESEM study was utilized to evaluate the cluster size.

Since the film material is of semiconductor nature and it possesses smoke-like characteristics with clusters, it may be a potential material in the application area of solar cell provided it should have considerable porosity and transmissive property to pass solar radiation. The detailed study regarding the electrical conductivity of the specimens was made. Electrical conductivity of the films determined by two probe method along parallel and perpendicular directions of the withdrawal operation of film deposition, is in the range of 10^{-1} to 10^{-4} Siemens cm^{-1} which is quite high with respect to commonly used titania system for solar cell application [38]. Table 3 illustrates the electrical parameters of the different ITO films measured by two probe method. It is observed that the electrical conductivity of ITO-150 is relatively low which is possibly due to the formation of PVA-ITO clusters of relatively high dimensions as evident from the increase in the physical thickness and FTIR study which is contrary to the PVP-ITO system [39]; the basic reason may be the difference in the decomposition temperature of the binders [7]. ITO-400 possessed the highest electrical conductivity. Electrical parameters of this sample were also determined by four probe Van der Pauw method. Here the electrode positions are designated as A, B, C and D placed 1 cm apart along the corners of a 1×1 cm^2 film surface. The potential difference between two electrodes in two opposite directions are given in Table 4 and their average values have been utilized to evaluate Hall mobility, carrier concentration, resistivity, conductivity and sheet resistance

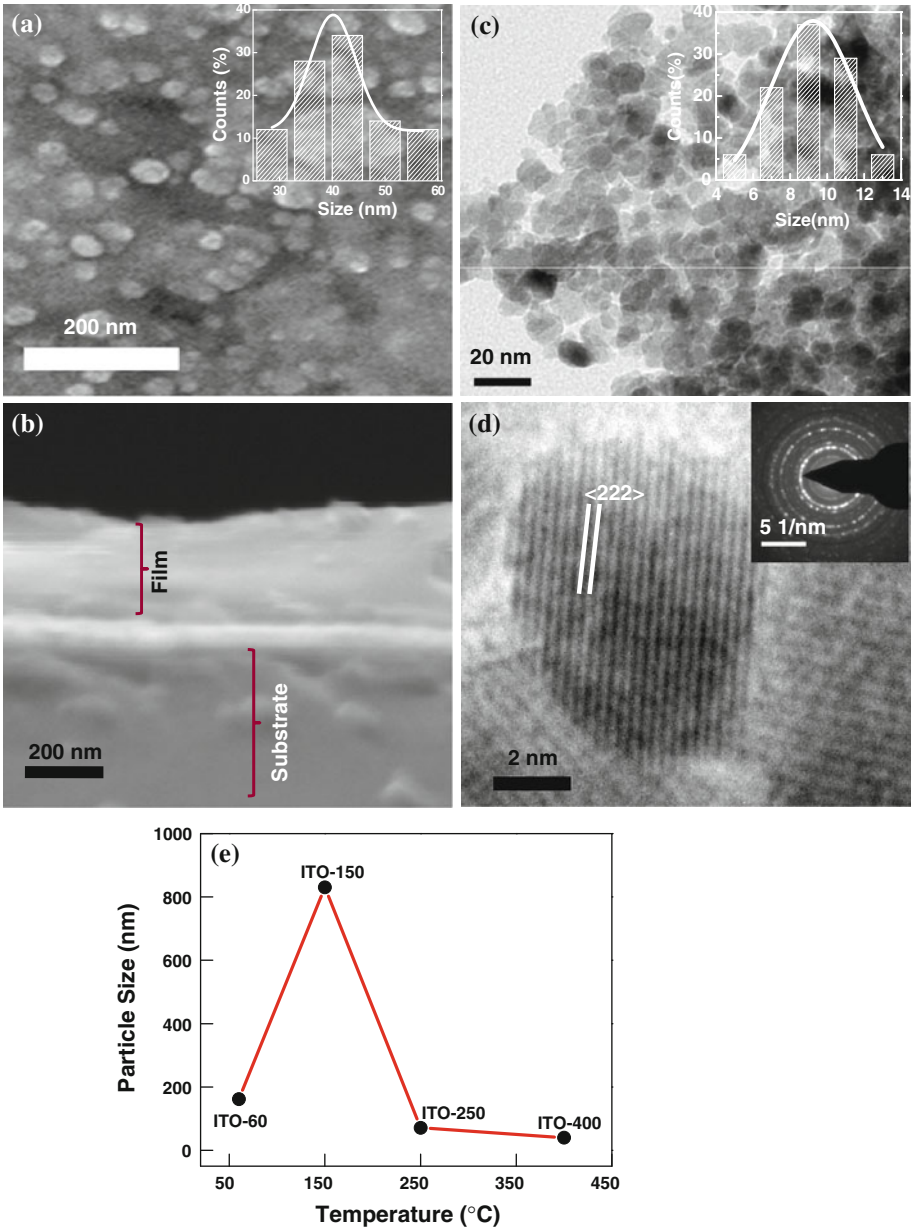

Fig. 10 **a** FESEM image of ITO-400 showing the film surface; *inset* shows histogram of particle size distribution with average size of ~40 nm. **b** Cross-sectional FESEM image of smoke-like ITO-400. **c** TEM image of ITO-400; *inset* shows histogram of particle size distribution with average size of ~9 nm; **d** lattice fringe by HRTEM showing (222) crystal plane; *inset* shows the ED pattern; **e** graphical representation of the average cluster sizes of the smoke-like ITO films against temperature

Table 3 Electrical parameters of different ITO films measured by two probe method along the parallel and perpendicular directions of withdrawal operation of film deposition

Specimen	Along the parallel direction of withdrawal operation of film deposition			Along the perpendicular direction of withdrawal operation of film deposition		
	Sheet resistance (Ω/□)	Resistivity (Ω cm)	Electrical conductivity (Siemens cm^{-1})	Sheet resistance (Ω/□)	Resistivity (Ω cm)	Electrical conductivity (Siemens cm^{-1})
ITO-60	8×10^6	462.4	2.16×10^{-3}	6×10^6	346.8	2.88×10^{-3}
ITO-150	18×10^6	2185.2	4.58×10^{-4}	26×10^6	3156.4	3.17×10^{-4}
ITO-250	4×10^6	146.0	6.85×10^{-3}	3×10^6	109.5	9.13×10^{-3}
ITO-400	14×10^4	3.5	2.86×10^{-1}	19×10^4	4.8	2.08×10^{-1}

(Table 5). The carrier concentration and Hall mobility of the system are not as good as those of ITO films [40], but these values are significant if compared with those values for porous Titania system [38]. The four probe measurement system could not be utilized for the other specimens as these show relatively high resistivity.

Table 4 Electrode potential difference between two probes of the four-probe system measured by Van der Pauw method (Input current, 1.0021 μA; applied magnetic field, 0.51 T)

V_{AB} (mV)	V_{BC} (mV)	V_{AC} (mV)	V_{CD} (mV)	V_{DA} (mV)	V_{BD} (mV)
−44.11	−78.98	−34.37	−44.31	−78.34	−34.56
+44.67	+79.43	+35.26	+44.50	+79.43	+35.04

In the four probe, the electrode positions are designated as A, B, C and D with 1 cm apart along the corners of a 1 × 1 cm^2 film surface of a typical system, ITO-400; voltage difference between two electrodes in two opposite directions indicated as + and − sign are given in this Table and their average value have been utilized to evaluate mobility, carrier concentration, resistivity, conductivity and sheet resistance (Table 5)

Table 5 Electrical parameters of ITO-400 determined from the data obtained in Table 4

Hall mobility (cm^2/Vs)	Carrier concentration (cm^{-3})	Resistivity (Ω cm)	Conductivity (Siemens cm^{-1})	Sheet resistance (Ω/□)
0.22	4.3×10^{18}	6.79	1.47×10^{-1}	27×10^4

The four probe measurement system could not be utilized for the other specimens as these show relatively high resistivity

Table 6 Adherence test data: % transmission and % reflection at 550 nm before and after the application of 3 M-Scotch tape and removal of material after the application of tape measured in terms of physical thickness

Specimen	No. of applications of tape	% Transmission before application of tape	% Transmission after application of tape	% Reflection before application of tape	% Reflection after application of tape	Removal of material in terms of thickness (Å)
ITO-60	100	83.3	87.3	5.2	5.7	∼100
ITO-150	100	82.9	85.7	5.0	5.6	∼75
ITO-250	100	78.8	79.2	7.1	7.3	∼52
ITO-400	100	83.2	83.6	6.3	6.7	∼25

To understand the mechanical durability of the coatings, the adhesion between the coating and the glass substrate was performed by the 3 M-Scotch-tape test. It was observed that no deterioration or damage of the coatings takes place due to hundred times application of the tapes. However, loss of very small fraction of the materials from the surface takes place for the samples heated at relatively low temperature where it may be presumed that anchoring of the coating material with the substrate did not occur considerably. This loss was examined ellipsometrically. The optical performance (% transmission and % reflection) at 550 nm was also executed to understand its effect with loss of surface materials. The loss of thickness due to application of tapes is in the range of ∼20–100 Å. The specimen ITO-400 is more stable and its change in optical performance is in the range of instrumental error. Table 6 reflects the adherence test data.

Conclusion

Porous and smoke-like ITO coating has been developed onto glass from the smoke-like gel layer. Incorporation of PVA in the precursor solution of hydrated indium nitrate and tin chloride has led to the formation of wettable precursor sol which develops smoke-like films on glass. Retention of smoke-like feature was observed even in the oxide form at 400 °C having porous bed of ITO with nanoclusters size range of 30–40 nm. The sequential steps of gel to oxide transformation of ITO system have been analysed by TG/DTA and FTIR study. Physical thickness of the final product is ∼250 nm and it is transparent (∼80%) in the solar radiation region. Application of smoke-like multilayer which is in progress would help to prepare a component of relatively high thickness of semiconducting nanoparticles. This may be utilised as dye/quantum dot (QD) absorber in solar cell systems. As the electrical conductivity of the smoke-like ITO film is considerably high with respect to that of commonly used Titania in solar cell, this may be used as an effective alternative of Titania system in future.

Acknowledgements The authors wish to acknowledge the Director, CGCRI for permission to publish this work. One of the authors (ND) thanks Board of Research in Nuclear Science (BRNS), Govt. of India for offering her SRF fellowship.

References

1. Biswas PK, De A, Dua LK, Chkoda L (2006) Appl Surf Sci 253:1953
2. Dwyer CO, Szachowicz M, Vimberga G, Lavayen V, Newcomb SB (2009) Nat Nanotechnol 4:239

3. Pocas LC, Nogueira SL, Nobuyasu RS, Dalkiranis GG, Pires MJM, Tozoni JR, Silva RA, Marletta A (2011) J Mater Sci 46:2644. doi:10.1007/s10853-010-5119-7
4. Straue N, Rauscher M, Walther S, Faber H, Roosen A (2009) J Mater Sci 44:6011. doi:10.1007/s10853-009-3804-1
5. Park IS, Lee E, Manthiram A (2009) J Electrochem Soc 157:B 251
6. Yumoto H, Inoue T, Sako T, Nishiyama K (1999) Thin Solid Films 345:38
7. Kundu S, Biswas PK (2005) Chem Phys Lett 414:107
8. Arachchige IU, Brock SK (2007) Acc Chem Res 40:801
9. Gao X, Nie S (2003) Trends Biotechnol 21:371
10. Gao X, Cui Y, Levenson RM, Chung LWK, Nie S (2004) Nat Biotechnol 22:969
11. Kalyanasundaram K, Gratzel M (1997) Proc Indian Acad Sci (Chem Sci) 109:447
12. Wong MS, Lee MF, Chen CL, Huang CH (2010) Thin Solid Films 519:1717
13. Singh HK, Agarwal DC, Chavhan PM, Mehra RM, Aggarwal S, Kulriya PK, Tripathi A, Avasthi DK (2010) Nucl Instrum Methods Phys Res B 268:3223
14. Lin H, Jin T, Dmytruk A, Saito M, Yazawa T (2004) J Photochem Photobiol A 164:173
15. Aksu Y, Frasca S, Wollenberger U, Matthias D, Thomas A (2011) Chem Mater 23:1798
16. Sujatha Ch, Rao MG, Uthanna S (2002) Mater Sci Eng B 94:106
17. Wang GJ, Chen HT (2009) Curr Nanosci 5:297
18. Yong TK, Tou TY, Teo BS (2005) Appl Surf Sci 248:388
19. Maruyama T, Fukui K (1991) Thin Solid Films 203:297
20. Rozati SM, Ganj T (2004) Renew Energ 29:1671
21. Minami T (2005) Sci Technol 20:S35
22. Aegerter MA, Puetz J, Gasparro G, Al-Dahoudi N (2004) Optical Mater 26:155
23. Epifani M, Diaz R, Arbiol J, Siciliano P, Morante JR (2006) Chem Mater 18:840
24. Assender HE, Windle AH (1998) Polymer 39:4303
25. Wang H, Lu X, Zhao Y, Wang C (2006) Mater Lett 60:2480
26. Bunn CW (1948) Nature 161:929
27. Colvin BG (1974) Nature 248:756
28. Kim SS, Choi SY, Park CU, Jin HW (1999) Thin Solid Films 347:155
29. Soloveva A, Zhdanov V (1985) Inor Mater (Engl Transl) 21:828
30. Mansur HS, Orifice RL, Mansur Alexander AP (2004) Polymer 45:7193
31. Souza ECC, Rey Q, Muccillo ENS (2009) Appl Surf Sci 255: 3779
32. Kim CO, Hong SY, Kim M, Park SM, Park JW (2004) J Colloid Interface Sci 277:499
33. Zhou XY, Jia DM, Cui YF, Xie AD (2009) J Reinf Plast Comp 28:2771
34. Chena SG, Li CH, Xionga WH, Liub LM, Wang H (2004) Mater Lett 58:294
35. Pramanik NC, Das S, Biswas PK (2002) Mater Lett 56:671
36. Lia S, Qiaoa X, Chena J, Wanga H, Jiaa F, Qiu X (2006) J Cryst Growth 289:151
37. Sato T (2005) J Therm Anal Calorim 82:775
38. Konenkamp B, Henninger R, Hoyer P (1993) J Phys Chem 97: 7328
39. Koniger T, Munstedt H (2009) J Mater Sci 44:2736. doi:10.1007/s10853-009-3357-3
40. Biswas PK, De A, Pramanik NC, Chakraborty PK, Ortner K, Hock S, Korder S (2003) Mater Lett 57:2326